

Desing of in Dual-Band synchronus Rectifier for High-Power Wireless Power Transmission Sytsem

Jianwei Zhou^{ID}, Guohua Liu^{ID}, *Member, IEEE*, Zhiwei Zhang^{ID}, *Member, IEEE*, and Yuezhi Wu^{ID}

Abstract—This letter propose a dual band-synchronous rectifier based on GaN transistors. To improve the efficiency of the rectifier a dual frequency phase-shifting network analyzed based on the positive and negative polarity modes of the rectifier. Then, the phase shift difference between any two frequencies are realized using a phase-shifting structure consisting of L and T-types networks. A high-efficiency dual band GaN synchronous rectifier operating at 0.905 and 2.4 GHz is the fabricated. In addition a high-power wireless power transmission experimental system was constructed using horn antennas. The system consist of a dual-band synchronous rectifier, a broadband power amplifier (PA), and a pair of waveguide input type standard gain horn antennas. Measurement results verifies the feasibility of the proposed system.

Index Terms—Dual band, GaN, synchronus rectifier, wireless power transmission system..

I. INTRODUCTON

WITH the development of wireless powertransmission technology, an emerging and market-valuable wireless charging field has been widely exploited [1], including drone charging [2], electric vehicles [3], and RFID [4]. Energy harvesting systems consisting of of-diode rectifiers have been widely reported [5], [6], [7], [10], [11]. However, the limited power capacity of diodes makes it difficult to meet the high-power requirements of applications, such as drone charging [12], [13]. Therefore, synchronous rectifiers based on GaN transistors are proposed [14], [15], [16], [17], and the power handling capacity of this rectifier can reach more than 10W, which is in line with the current demand for high-power application scenarios. An intentionally sourced wireless power transfer system consisting of a transistor rectifier and an antenna could potentially be used for space solar power stations or where wired power is not readily available. The system operates in the industrial, scientific and medical (ISM) band to avoid interference with mobile communications.

The multiband rectifier in the ISM can support high-performance power transfer, and it is able to reduce the size and mitigate the costs. There are only a few sporadic reports on transistorized multiband synchronous rectifiers. In [18], depending on the direction of the output voltage, the

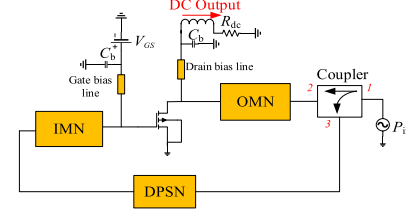


Fig. 1. Topology of the synchronous rectifier.

synchronous rectifiers has two modes of operation, positive and negative polarity modes. Synchronous rectifiers operating in negative polarity mode have the possibility of gate current generation, and there is a risk of transistor destruction. Therefore, to prevent disable to the power devise, a positive polarity mode dual-band synchronous rectifier is designed. In addition, an dual-band phase-shifting structure is proposed, which utilizes the composition of L-type and T-type networks to realize the phase-shifting difference between any two frequencies. Finally, a rectifier operating both 0.905 and 2.4 GHz were fabricated. This rectifier are used in the receiving end of the high-power wireless power transmission system.

II. ANALYSIS OF THE PROPOSED RECTIFIER

According to the principle of time-reversal duality, the input of the rectifier is the output of the PA (power amplifier), and the drain bias terminal of the amplifier becomes the dc output port of the rectifier. The Fig. 1 shows the diagram of the proposed dual-band rectifier. The dual-band phase-shifting network (DPSN) controls the drain-gate phase shift, which ensure

According to the positive and negative polarity modes of the synchronous rectifier, two operating frequencies f_1 and f_2 are set, respectively, and the phase shift difference $\varphi = \pi$ of the phase shift network in the above two operating modes. The phase shift difference of π makes the rectifier highly efficient [19]. In this design, the operating frequencies f_1 and f_2 of the synchronous rectifier are set in positive polarity mode, and a frequency f_0 is selected between the two frequencies operating in the negative polarity mode

$$\varphi_{f_1} - \varphi_{f_0} = \pi \quad (1)$$

$$\varphi_{f_0} - \varphi_{f_2} = \pi. \quad (2)$$

Then

$$\varphi_{f_1} - \varphi_{f_2} = 2\pi. \quad (2)$$

The phase shift network of the dual-band rectifier has a phase difference of 360° at f_1 and f_2 .

Manuscript received 26 July 2024; accepted 3 August 2024. This work was supported in part by Zhejiang Provincial Science and Technology Plan under Project 2024C01076. (Corresponding author: Guohua Liu.)

The authors are with the School of Electronics and Information, Hangzhou Dianzi University, Hangzhou 310018, China (e-mail: zjw@hdu.edu.cn; ghliu@hdu.edu.cn; 2361051379@qq.com; wuyuezhi@hdu.edu.cn).

Color versions of one or more figures in this letter are available at <https://doi.org/10.1109/LMWT.2024.3440336>.

Digital Object Identifier 10.1109/LMWT.2024.3440336

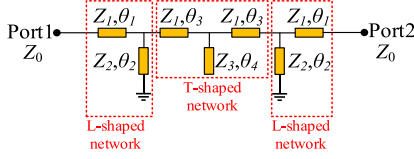


Fig. 2. Phase shift network.

As shown in the Fig. 2, the DPSN consists of two L-shaped networks and one T-shaped network. The structure achieves a 180° phase shift difference on f_1 and f_2 and it corresponds to the polarity mode of the rectifier [20]. Its ABCD parameters and phase shift are, respectively

$$\begin{bmatrix} A & B \\ C & D \end{bmatrix}_P = \begin{bmatrix} A_1 & B_1 \\ C_1 & D_1 \end{bmatrix}_L \begin{bmatrix} A_2 & B_2 \\ C_2 & D_2 \end{bmatrix}_T \begin{bmatrix} A_3 & B_3 \\ C_3 & D_3 \end{bmatrix}_L \quad (4)$$

$$\varphi_x = -\tan^{-1} \left[\frac{B_x/Z_0 + C_x Z_0}{j(A_x + D_x)} \right] \quad (5)$$

where Z_0 is the characteristic impedance of the system port.

According to the dual-band theory, the phase shift of the two frequencies can be expressed as

$$\frac{\varphi_{f_1}}{f_1} = \frac{\varphi_{f_2}}{f_2}. \quad (6)$$

Therefore, the phase shift difference between the two frequency bands is

$$\varphi = (\varphi_1 + \varphi_2 + \varphi_3)|_{f=f_1} - (\varphi_1 + \varphi_2 + \varphi_3)|_{f=f_2} = 2\pi. \quad (6)$$

Further combining (3) to (7), the phase shift difference φ at f_2 varies as a function of impedance Z_1 – Z_3 and angle θ_1 – θ_4 in Fig. 2 can be deduced. Function φ is plotted, as shown in Fig. 3. It can be observed that by setting the parameters appropriately, the desired value of φ can be obtained.

From Fig. 3(a) and (b), to ensure that the phase shift network has a phase shift difference of 360° at two frequencies, we can obtain the range of values of impedance Z_1 – Z_3 as 20 – 40Ω , 30 – 70Ω , and 40 – 70Ω , respectively. From Fig. 3(c)–(f), we can estimate that the range of values of θ_1 – θ_4 are 70° – 85° , 60° to 100° , 60° to 85° , and 30° – 80° , respectively. In addition, different combinations of parameters can lead to variations in the phase shift φ . When θ_1 takes the value of 72° , it satisfies θ_1 in Fig. 3(d), while it cannot fit φ in the Fig. 3(c). Therefore, the actual value of the parameter may be slightly out of the range

III. DESIGN AND MEASUREMENT OF DUAL-BAND SYNCHRONOUS RECTIFIER

Rectifier design steps are as follows: first, it is determined that both bands of the dual-band rectifier operate in the positive polarity mode. Their operating frequencies f_1 and f_2 are 0.905 and 2.4 GHz, respectively. Then, the dual-band phase shift network is determined, as shown in the Fig. 2, which consists of two L-type and T-type networks. After that, the phase shift difference φ of the network at the two frequencies is calculated based on the determined phase shift network. Finally, the function φ is plotted versus impedance Z_1 – Z_3 and θ_1 – θ_4 shown in the Fig. 3. Based on the above design methodology, the values of Z_1 – Z_3 and θ_1 – θ_4 can be obtained as 35 , 60 , and 50Ω and 66° , 87° , 90° and 43° , respectively.

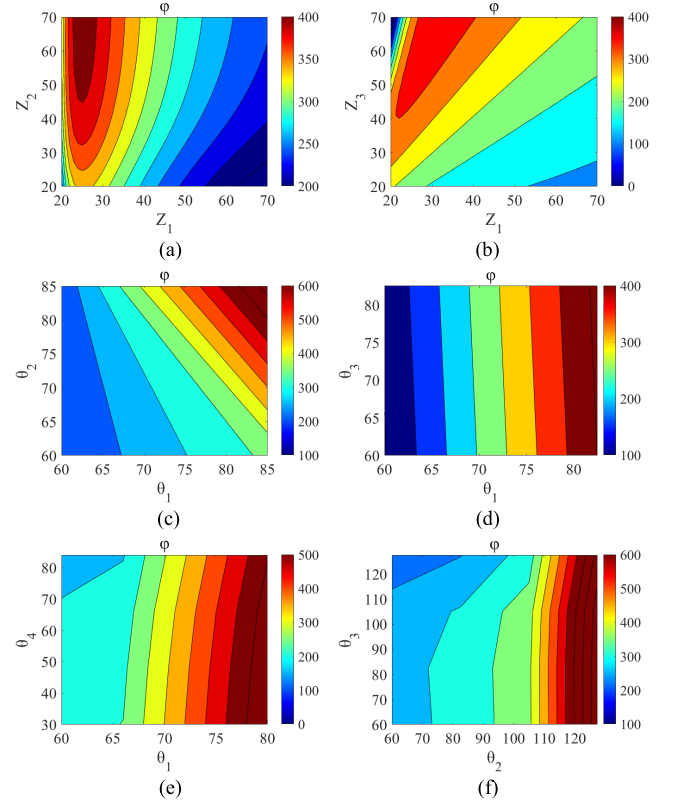


Fig. 3. Phase shift difference φ versus impedance Z_1 – Z_3 and angle θ_1 – θ_4 . (a) $Z_3 = 50 \Omega$. (b) $Z_2 = 60 \Omega$. (c) $\theta_3 = 90$ and $\theta_4 = 45^\circ$. (d) $\theta_2 = 90^\circ$ and $\theta_4 = 45^\circ$. (e) $\theta_2 = 90$ and $\theta_3 = 90$. (f) $\theta_1 = 70^\circ$ and $\theta_4 = 45^\circ$.

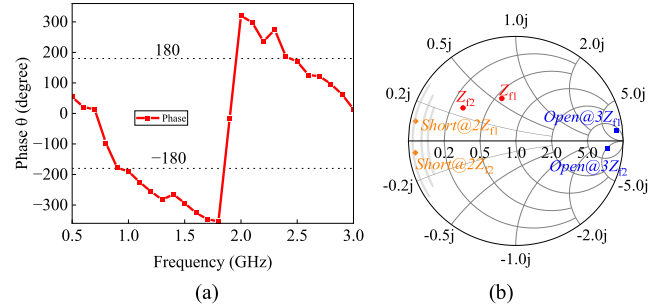


Fig. 4. Simulated (a) phase shift and (b) load impedances.

The values of φ_{f_1} and φ_{f_2} in Fig. 4(a) are -180° and 180° , so the value φ is 360° , which is in accordance with the design theory.

In this letter, the Class-F amplifier theory is used to design the input and output impedance of the transistor. The simulated load impedances are finalized as $Z_{f1} = (28.44 + j28.2) \Omega$ and $Z_{f2} = (14.2 + j13.6) \Omega$ by load pulling. Meanwhile, the harmonic control block in the Fig. 5 uses TL_1 – TL_6 to satisfy the desired harmonic impedance condition of ideal Class-F operation mode. For the second-harmonic control,

transmission lines $TL_1 + TL_3 = \lambda/4$ at f_1 and $TL_1 + TL_2 = \lambda/8$ at f_2 . For the third-harmonic control, transmission lines $TL_1 + TL_4 + TL_5 = \lambda/6$ at f_1 and $TL_1 + TL_4 + TL_6 = \lambda/6$ at f_2 . After optimization, the simulated load impedance is shown in Fig. 4(b), indicating that the simulated load impedances Z_{f1} and Z_{f2} are close to the theoretical impedance. Moreover, the second harmonic is short, and the third harmonic is open, which is in accordance with the Class-F theory. An approximation of the fundamental source

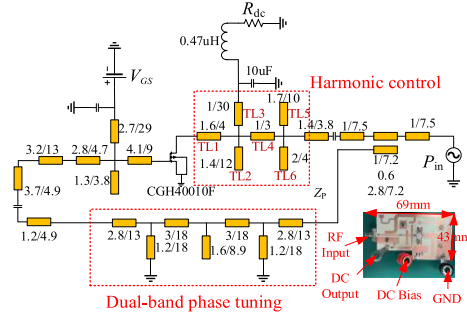


Fig. 5. Rectifier circuit schematic with distributed parameters and photograph.

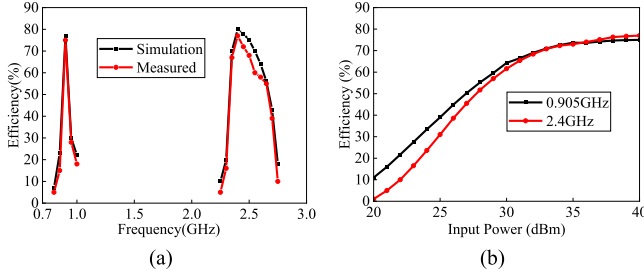


Fig. 5. Effect of (a) frequency and (b) input power changes on efficiency at 0.905 and 2.4 GHz.

impedance at frequencies can be obtained from the source pull as $(2.7 - j * 3.8) \Omega$ and $(3.2 - j * 4.2) \Omega$.

To verify the effectiveness of the proposed method, we designed a dual-band synchronous rectifier based on Rogers 4350b substrate ($\epsilon_r = 3.66$, and $h = 30$ mil) with CGH40010F GaN HEMT. The complete rectifier circuit is shown in Fig. 5

In this design, the gate bias and RF input power of the rectifier are -3.5 V and 40 dBm, respectively. The relationship between rectification efficiency and frequency is shown in Fig. 6(a). At an input power of 40 dBm, the peak efficiency is 75% with f_1 and 77% with f_2 . The input power sweep at two frequencies is shown in Fig. 6(b). As can be seen that in the two frequency bands, the rectifier has a rectification efficiency above 60% with an input power greater than >30 dBm.

IV. DESIGN AND MEASUREMENT OF WIRELESS POWER TRANSMISSION SYSTEM

To verify the effectiveness of the above design methodology, a wireless power transmission system was designed for validation. Fig. 7(a) shows a photograph of the wireless power transmission system test scenario. The PA in the photograph is a broadband PA based on the CGH40025F with an output power of 44 dBm at 2.4 GHz. The transmit and receive antennas are waveguide-input standard gain horn antennas (HD-26SGAH10N), which operates from 2.17 to 3.3 GHz with a gain of 10 dBi. Considering the generation of reflected waves during testing, add an isolator between PA and antenna, which has a loss of 1.6 dB.

In Fig. 7(b), η represent the system efficiency, η_1 denotes the antenna transmission efficiency, η_2 indicate the rectifier efficiency, D_r are the distance between the two antennas, P_T means the antenna transmit power, P_R demonstrate the antenna receive power, and P_{rec} represents the rectifier output power.

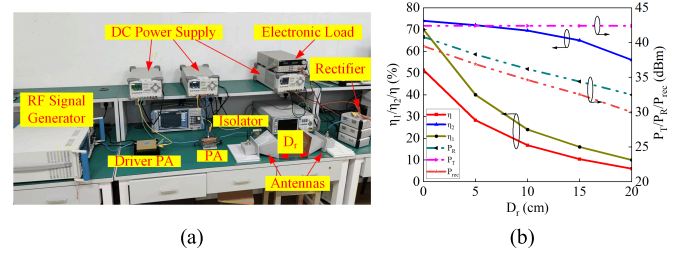


Fig. 7. Wireless power transmission system. (a) Test scenario diagram. (b) Effect of D_r changes on efficiency and power at 2.4 GHz.

TABLE I
PERFORMANCE COMPARISON WITH RECTIFIERS

Ref	Device	Freq (GHz)	Pin (dBm)	Efficiency (%)	Area(λ^*)@ Freq(GHz)	SE*
[5]	Schottky diode	5.8	10	52.48	$0.7\lambda \times 0.8\lambda @ 5.8$	NO
[7]	Schottky diode	1.7/2.4/3.8/5.3	0	72/66/70/68	$\lambda \times 1.1\lambda @ 1.7$	NO
[13]	Schottky diode	0.915/2.45	17	74.9/71.2	$0.74\lambda \times 0.27\lambda @ 0.915$	NO
[17]	GaN HEMT	1.17/2.4	40	77/75	$0.2\lambda \times 0.2\lambda @ 1.17$	NO
[18]	GaN HEMT	1.8	40	77	NO	NO
[19]	GaN HEMT	1.9/2.4	40	75/76	$0.21\lambda \times 0.3\lambda @ 1.9$	NO
This Work	GaN HEMT	0.905/2.4	40	75/77	$0.2\lambda \times 0.13\lambda @ 0.905$	Yes

*: System efficiency

Measure the antenna P_R individually using a spectrum analyzer to obtain the measured value η_1 shown in Fig. 7(b), and it was found that when P_T was fixed, P_R decreased by 2 dB for every 5 cm increase in D_r . When P_T is 42.4 dBm, the antenna received power decreases rapidly as D_r increases, resulting in an inefficient system. When $D_r = 0$, the system efficiency reaches a maximum value of 51.4%.

The Table I list the performance comparison of some related rectifiers. We can see that the proposed rectifier exhibits the higher input power capacity compared to the rectifiers using diodes. When compared with transistor-based rectifier, this work has highest frequency ratio. In addition, wireless power transmission system measurements were performed on the designed rectifier. However, the inefficiency of the system can be due to the following possible reasons: one is small receiving area of the receiving antenna cannot collect all transmitted power. The other is impedance mismatch between the rectifier and the antenna.

V. CONCLUSIONS

This letters presents a dual-band synchronous rectifier for high-power wireless power transmission systems. When the input power is 40 dbm, the efficiency of the rectifier at two frequencies is 75% and 77%, respectively. To verify the feasibility of the system, a test platform was built. The experimental results show that the wireless transmission is successfully realized at 2.4 GHz. In the future, array antennas will be designed replace horn receiving antennas to improve the transmission efficiency between antennas. In addition, wireless energy transfer systems will be conceived for use in unmanned aerial vehicles, where the receiver section replaces the solid-state battery, thus reducing the overall weight of the unmanned aerial vehicles and increasing its range.

REFERENCES

- [1] X. Lu, P. Wang, D. Niyato, D. I. Kim, and Z. Han, "Wireless charging technologies: Fundamentals, standards, and network applications," *IEEE Commun. Surveys Tuts.*, vol. 18, no. 2, pp. 1413–1452, 2nd Quart., 2016.
- [2] Y. Gu, J. Wang, Z. Liang, and Z. Zhang, "A wireless in-flight charging range extended PT-WPT system using S/single-inductor-double-capacitor compensation network for drones," *IEEE Trans. Power Electron.*, vol. 38, no. 10, pp. 11847–11858, Oct. 2023.
- [3] Y. Zhang et al., "Misalignment-tolerant dual-transmitter electric vehicle wireless charging system with reconfigurable topologies," *IEEE Trans. Power Electron.*, vol. 37, no. 8, pp. 8816–8819, Aug. 2022.
- [4] Y. Yao, J. Wu, Y. Shi, and F. F. Dai, "A fully integrated 900-MHz passive RFID transponder front end with novel zero-threshold RF-DC rectifier," *IEEE Trans. Ind. Electron.*, vol. 56, no. 7, pp. 2317–2325, Jul. 2009.
- [5] W. Hui, Y. Guo, and X. Zhao, "Polarization-tunable microstrip antenna based on double V-Type metamaterials cover for microwave energy harvesting," *IEEE Antennas Wireless Propag. Lett.*, vol. 22, pp. 729–733, 2023.
- [6] Y. Shi and Y. H. Nan, "Hybrid power harvesting from ambient radiofrequency and solar energy," *IEEE Antennas Wireless Propag. Lett.*, vol. 21, pp. 2382–2386, 2022.
- [7] Z.-J. He, L.-L. Qiu, P. Zhang, Y. Liu, S. Huang, and L. Deng, "A high efficiency rectifying metasurface with four operating bands," *IEEE Antennas Wireless Propag. Lett.*, vol. 22, no. 10, pp. 2387–2391, Jun. 2023.
- [8] M. A. Halimi, T. Khan, S. K. Koul, and S. R. Rengarajan, "A dual-band rectifier using half-wave transmission line matching for 5G and Wi-Fi bands RFEH/MPT applications," *IEEE Microw. Wireless Technol. Lett.*, vol. 33, no. 1, pp. 74–77, Jan. 2023.
- [9] M. A. Halimi, D. Surender, T. Khan, A. A. Kishk, and S. R. Rengarajan, "A multisteped transmission line matching strategy based triple-band rectifier for RFEH/WPT applications," *IEEE Microw. Wireless Compon. Lett.*, vol. 32, no. 8, pp. 1007–1010, Aug. 2022.
- [10] M. A. Halimi, T. Khan, M. Palandoken, A. A. Kishk, and Y. M. M. Antar, "Rectifier design challenges for wireless energy harvesting/wireless power transfer systems: Broadening bandwidth and extended input power range," *IEEE Microw. Mag.*, vol. 24, no. 6, pp. 54–67, Jun. 2023.
- [11] M. A. Halimi, T. Khan, A. A. Kishk, and Y. M. M. Antar, "Rectifier circuits for RF energy harvesting and wireless power transfer applications: A comprehensive review based on operating conditions," *IEEE Microw. Mag.*, vol. 24, no. 1, pp. 46–61, Jan. 2023.
- [12] M. Huang et al., "Single- and dual-band RF rectifiers with extended input power range using automatic impedance transforming," *IEEE Trans. Microw. Theory Techn.*, vol. 67, no. 5, pp. 1974–1984, May 2019.
- [13] J. Liu, X. Y. Zhang, and Q. Xue, "Dual-band transmission-line resistance compression network and its application to rectifiers," *IEEE Trans. Circuits Syst. I, Reg. Papers*, vol. 66, no. 1, pp. 119–132, Jan. 2019.
- [14] Z. Zhang, C. Gu, Z. Cheng, and X. Xuan, "Design a GaN HEMT-based broadband high-efficiency rectifier using a wideband phase shift structure," *IEEE Microw. Wireless Technol. Lett.*, vol. 33, no. 6, pp. 751–754, Jun. 2023.
- [15] Z. Zhang, C. Gu, Z. Cheng, and X. Xuan, "A high-power capacity transistor-based rectifier with wide input power range," *IEEE Microw. Wireless Technol. Lett.*, vol. 33, no. 6, pp. 747–750, Jun. 2023.
- [16] F. You, S.-W. Dong, Y. Wang, S. Zhang, X. Yu, and S. He, "Design of a self-driving transistor-based RF-DC converter based on optimized harmonic-tuned rectification waveforms," *IEEE Trans. Microw. Theory Techn.*, vol. 68, no. 10, pp. 4433–4444, Oct. 2020.
- [17] M. A. Hoque et al., "Highly efficient multiband harmonic-tuned GaN RF synchronous rectifier," *IEEE Trans. Microw. Theory Techn.*, vol. 71, no. 11, pp. 5060–5072, Nov. 2023.
- [18] S. N. Ali, T. Johnson, and D. Heo, "DC polarity control in radio frequency synchronous rectifier circuits," *IEEE Microw. Wireless Compon. Lett.*, vol. 27, no. 12, pp. 1107–1109, Dec. 2017.
- [19] Z. Zhang, V. Fusco, Z. Cheng, N. Buchanan, and C. Gu, "A transistor-based dual-band high-efficiency rectifier with dual-polarity modes," *IEEE Microw. Wireless Compon. Lett.*, vol. 32, no. 2, pp. 169–172, Feb. 2022.
- [20] Q. Dong, Y. Wu, W. Chen, Y. Yang, and W. Wang, "Single-layer dual-band bandwidth-enhanced filtering phase shifter with two different predetermined phase-shifting values," *IEEE Trans. Circuits Syst. II, Exp. Briefs*, vol. 68, no. 1, pp. 236–240, Jan. 2021.